Fabrication and characterization of 20 nm planar nanofluidic channels by glass–glass and glass–silicon bonding

Pan Mao[a] and Jongyoon Han*[bc]

Received 28th February 2005, Accepted 6th June 2005
First published as an Advance Article on the web 30th June 2005
DOI: 10.1039/b502809d

We have characterized glass–glass and glass–Si bonding processes for the fabrication of wide, shallow nanofluidic channels with depths down to the nanometer scale. Nanochannels on glass or Si substrate are formed by reactive ion etching or a wet etching process, and are sealed with another flat substrate either by glass–glass fusion bonding (550 °C) or an anodic bonding process. We demonstrate that glass–glass nanofluidic channels as shallow as 25 nm with low aspect ratio of 0.0005 (depth to width) can be achieved with the developed glass–glass bonding technique. We also find that silicon–glass nanofluidic channels, as shallow as 20 nm with aspect ratio of 0.004, can be reliably obtained with the anodic bonding technique. The thickness uniformity of sealed nanofluidic channels is confirmed by cross-sectional SEM analysis after bonding. It is shown that there is no significant change in the depth of the nanofluidic channels due to anodic bonding and glass–glass fusion bonding processes.

Introduction

Nanometer-scale fluidic structures have gained considerable attention in the last few years because they provide unique capability in biomolecular manipulation and control.[1] Nanofluidic structures with a critical size smaller than 100 nm can put a physical constraint on the biomolecules in solution, therefore controlling the molecules in a unique and useful way. So far, nanofluidic devices have found significant applications in biotechnology and medicine, including separation of biomolecules,[2,3] drug delivery,[4] and single molecule detection.[5–8] Also, the molecular stochastic motion and the fluidic properties are quite different within nanofluidic structures. Regular nanofluidic channels provide ideal experimental platforms for well-controlled, model-based study of molecular and fluidic transport processes in confined space.[9,10]

One critical issue in nanofluidics is the availability of reliable, reproducible fabrication strategies for nanometer-sized fluidic structures. Several fabrication strategies have been demonstrated so far. Turner *et al.*[11] used the monolithic sacrificial etching technique, combined with e-beam lithography, to generate ~50 nm fluidic obstructions. Cao *et al.*[12] used nanoimprint lithography and nonuniform deposition techniques to generate sealed nanochannels as small as 10 nm × 50 nm. These techniques will allow much flexibility in the possible shapes of the nanofluidic structures. However, they require relatively expensive nanolithography techniques to define their features. Furthermore, techniques based on the sacrificial layer etching[11,13] as well as thin, deposited capping layers, sometimes suffer from the residual stress and mechanical defects of the capping layers.

While one dimensional (1D) nanofluidic channels have been used to study the polymer dynamics in pseudo 1D nanochannels,[14,15] the sorting, filtering, and manipulation of biomolecules require confinement only in one dimension. Therefore, an easy alternative for such nanolithography-based techniques would be fabricating "shallow" channels, instead of "narrow" channels. This technique has been explored by Han and Craighead,[16] and successfully applied to the separation of large DNA molecules.[2,17] In this technique, a channel pattern is defined by photolithography on silicon substrate, and then etched for a short time (either by wet etching or reactive ion etching) to generate very shallow trenches. Then, anodic bonding[18] is used to bond a flat Pyrex glass wafer to the silicon substrate with the help of high electric field (400 ~ 800 V across the junction) and heat (typically 300 ~ 400 °C). This technique eliminates the need of nanolithography to build nanofluidic structures, while allowing the well-defined flat nanochannels with good control on the "pore size" (channel depth in this case). The channel depth can be controlled by tuning etch time of silicon or glass substrates, and the etch rate can also be slowed down (either by diluting wet etchant or de-optimizing the RIE conditions) to make the thickness control more precise. Also, nanochnannels made by this method are much more robust mechanically, since there is no issue related to the stress and fragility of thin capping layers.

While the fabrication of nanofluidic channels as thin as 30 nm has been achieved by Han,[19] the uniformity of the channel as well as the limit of this technique has never been characterized. Considering the strong electric field and high temperature employed in the bonding process, the nanochannel might sag and, as a result, the depth of the channel might change. Another drawback here is that the anodic bonding process generally requires Si and borosilicate glass substrate. In many applications, nanofluidic devices made out of all glass substrates are preferred over silicon due to its mechanical strength, optical transparency, and non-conductivity. One

[a]*Department of Mechanical Engineering, MA 02139, USA*
[b]*Department of Electrical Engineering and Computer Science, MA 02139, USA*
[c]*Biological Engineering Division, Massachusetts Institute of Technology, Cambridge, MA 02139, USA. E-mail: jyhan@mit.edu*

could potentially use the same method to fabricate shallow glass–glass nanofluidic channels, but the critical step here would be the glass–glass bonding process. A number of glass–glass direct bonding techniques, including low temperature and high temperature bonding, have been extensively studied and developed. Wang *et al.*[20] fabricated glass microchip devices with strong bonding and good channel sealing by employing sodium silicate as an adhesive layer at 90 °C. Huang *et al.*[21] used a UV-curable glue to achieve glass microchip bonding at room temperature. Sayah *et al.*[22] described two direct low temperature bonding techniques with epoxy gluing process and high pressure, respectively. Chiem *et al.*[23] reported a room-temperature bonding procedure based on rigorous cleaning. Recently, Jia *et al.*[24] achieved effective bonding of glass chips under a continuous flow of water at room temperature without the requirement of a clean-room facility. Usually, the low temperature bonding requires a rigorous cleaning procedure prior to bonding and the bonding strength could not be as large as high temperature bonding. Besides, the usage of adhesives or glue may clog the channels, especially for fabricating very shallow channels. In contrast to the low temperature bonding process, thermal fusion bonding at high temperature can provide good bonding strength and high bonding yield. Lin *et al.*[25] succeeded in sealing microfluidic channels on soda-lime glass at 580 °C for 20 min with a slight pressure applied. Fan *et al.*[26] achieved effective bonding between two Pyrex glass wafers at 640 °C after 6 hours. Although glass–glass bonding at high temperature (around 600 °C for Pyrex) can be achieved successfully with large bonding strengths, the channels tend to be distorted and even collapse since the glass material at high temperature will be softened. Therefore, most of the above high temperature bonding techniques are mainly used for fabricating relatively deep microchannels (~10 μm in thickness), and the applicability of the glass–glass fusion bonding technique for shallow nanofluidic channels has never been tested.

In this paper, we carefully investigated and characterized the applicability and limit of the substrate bonding techniques, both Si–glass anodic and glass–glass fusion bonding, in fabricating sub-100 nm deep nanofluidic channels. We designed a test pattern for nanochannels, which allowed us to identify the minimum aspect ratio of the channel (depth to width) achievable without inducing collapse. We also used scanning electron microscopy (SEM) imaging to examine the uniformity and deformation of the bonded nanofluidic channels. The minimum aspect ratio of the shallow nanochannel, as well as the ultimate limit of the techniques in generating sub-10 nm channels, was discussed.

Experimental

Chip layout

The photomask pattern was generated with the software L-Edit Pro Version 10 (Tanner EDA, CA) and transferred onto a high-quality chrome mask with a resolution of 1 μm (Microtronics Inc, PA). As shown in Fig. 1, the mask, full of 2 cm long parallel lines with various widths spaced at several microns from each other, was designed to make it easy to locate channels while doing SEM analysis. All the following

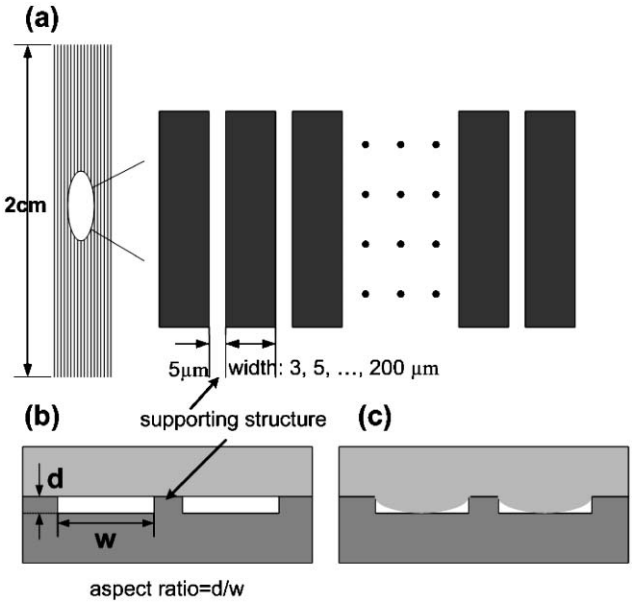

Fig. 1 (a) Layout of the test pattern consisting of an array of 2 cm long parallel lines with various widths spaced at 5 μm from each other. The width varies from 3 μm to 200 μm. (b) Schematic diagram of the cross-sectional nanochannels. (c) Failure or collapse of the nanochannel fabrication (cross-sectional view).

fabrication processes except the glass–glass bonding step were done in a class 100 cleanroom at MIT.

Fabrication of nanochannels on silicon substrate

A schematic diagram of the fabrication process is given in Fig. 2(A). Nanochannels with various widths and depths were patterned and etched into silicon wafers by photolithography and reactive ion etching, as described by Han *et al.*[16] It is straightforward to control the depth of the channel by adjusting etch parameters. The depth of the etched channels was measured by the profilometer (Prometrix P-10, KLA-Tencor Co., CA). After cleaning the substrate, a thermal oxide layer (400 nm thick) was grown to provide an electrical isolation between silicon substrate and fluid solution. Finally, the silicon devices were bonded to flat glass wafers (6″ PYREX or Borofloat, 0.5 mm thick, Sensor Prep Services Inc., IL) in the bonder machine (EV501, EV Group) by anodic bonding technique. The bonding process was carried out around half an hour at 350 °C with an applied voltage of 800 V, which is a widely used procedure for anodic bonding.

Fabrication of nanochannels on glass substrate

The fabrication steps are schematically shown in Fig. 2(B). Borosilicate glass (PYREX or Borofloat, Sensor Prep Services Inc., IL) wafers with a diameter of 150 mm, a thickness of 0.5 mm and double sides polished with 15 ~ 20 Å surface finish were used. Usually, an evaporated metal film or polysilicon/nitride layer is used as a wet-chemical etch mask for fabrication of microfluidic devices on glass substrate. Instead, in this study, a thin layer of photoresist (OCG 825) is used as an etch mask for borosilicate glass in the BOE

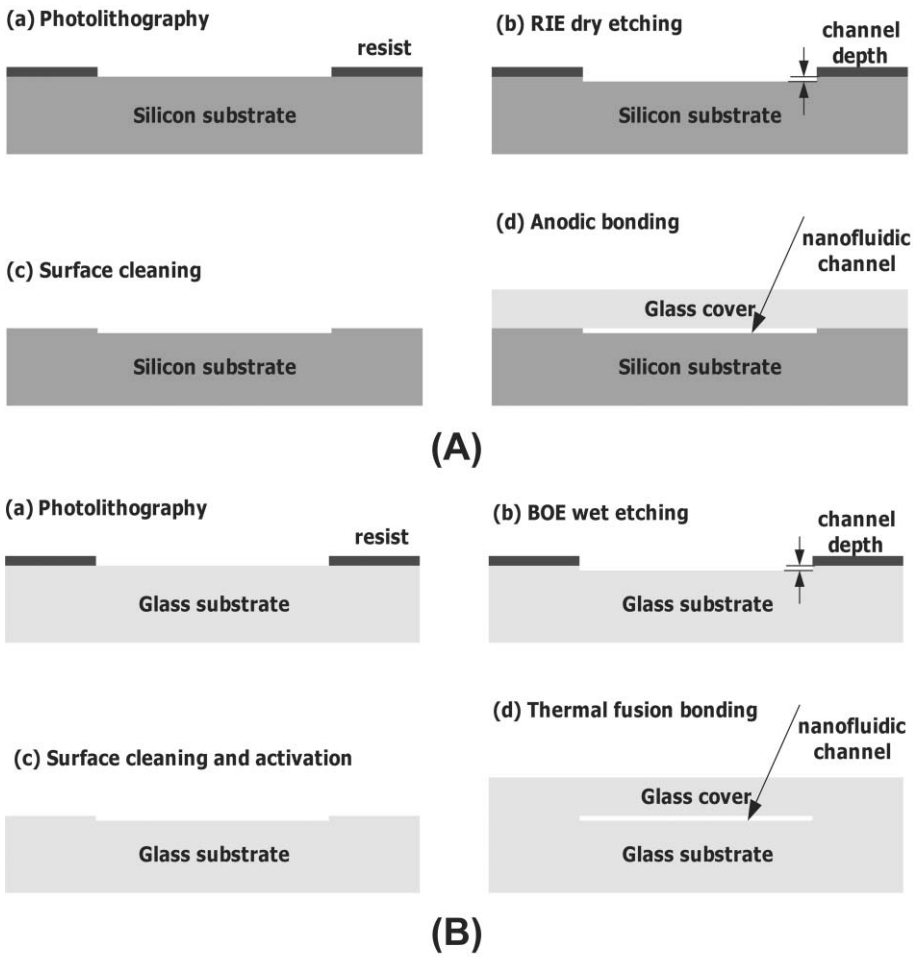

Fig. 2 Schematic description of nanochannel fabrication process on silicon substrate (A) and glass substrate (B).

etchant. The glass wafers were cleaned in a piranha solution (H_2SO_4(%):H_2O_2(%) = 3:1) for 10 min, rinsed in DI water and spun dry with nitrogen gas. The dehydration process was performed by baking the glass wafers at 120 °C for more than one hour in a convection oven. To improve the adhesion of the photoresist, the wafers were then vapor primed with hexamethyldisilazane (HMDS). The primer-treated substrates were coated with an OCG 825 positive resist, and soft baked at 95 °C for half an hour in a convection oven. After UV exposure, development and hardbake process, the thickness of the resist layer was about 1.2 μm, which can provide a survival time of resist in the BOE etchant long enough to achieve up to 600 nm thick channels.

Then, the glass substrate was immersed in a commercial buffered oxide etchant (BOE 7:1) without agitation. The depth of the nanofluidic channel can be well controlled by tuning the etching time. The remaining photoresist was removed in piranha solution after BOE etching. The etched depth was measured by P-10 as described above. A calibration of the etch rate of borosilicate glass without agitation in the commercial BOE etchant (7:1) at room temperature was done and the graph of the channel depth *versus* the etch time is given in Fig. 3. It is shown that BOE etches glass very fast in a short etching time (within 1 min) and then the etch rate reaches a stable speed of 24 nm min^{-1} over 12 min. This is most likely because borosilicate glass is a multicomponent mixture of SiO_2 and other metal oxides (Na_2O, CaO, MgO, and Fe_2O_3). The insoluble products will be present during etching and the formation of crystalline precipitates will hinder the etching process by preventing etchants from contacting the glass substrate while etching glass in a HF-containing solution.[25] The observed etch rate is much slower than 0.063 μm min^{-1} reported by Vossen and Kern.[27]

Finally, the etched glass substrate and another glass cover were cleaned in piranha solution for 10 min and then activated with 28% ammonium hydroxide at 50 °C for 30 min. After spin-drying, the two glass wafers were then carefully aligned and pressed together to make a spontaneous bonding, with about 5 lb weights (metal plate) placed on the top for a few hours or overnight. Finally thermal bonding was achieved by annealing (without weight or pressure) in a programmable furnace (Model BF51894C-1, Lindberg/Blue M, NC) at 550 °C for 12 ~ 18 hours with a ramp rate of 1.0 ~ 1.5 °C min^{-1} and a cooldown rate of 1.5 ~ 2.5 °C min^{-1}.

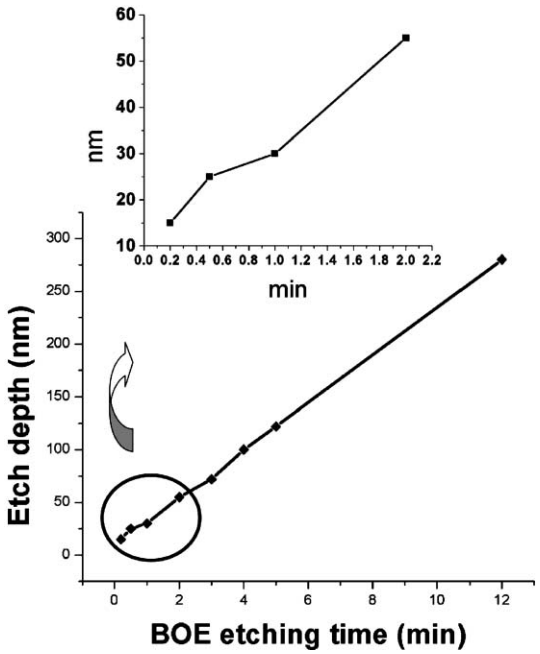

Fig. 3 The etched depth of nanofluidic channels as a function of etching time of glass without agitation in BOE (7:1) etchant. The stable etch rate is around 24 nm min^{-1}.

Results and discussion

Nanochannel fabrication by anodic bonding

The fabrication process on silicon substrate using anodic bonding technique is fairly standard, simple, and repeatable. We fabricated nanochannels with various widths and depths to investigate the limit of this fabrication technique in the normal bonding condition. Table 1 summarizes the result of the survival or collapse of the channels with various depths and widths by optical inspection. The optical micrograph of the typical success or failure of nanochannels is shown in Fig. 4. The channels turn from bright to gray when they collapse. Once its roof makes contact, a channel collapses quickly and completely due to the strong attractive interfacial surface force, except the narrow region along the edge.

Nanofluidic channels as thin as 20 nm with rather low aspect ratio (0.004, depth to width) have been achieved with this technique, which is smaller than the 30 nm nanofluidic channels reported by Han.[19] This result is significant since the aspect ratio of the nanochannel is much lower than the previous reports where several researchers described fabrication of nanochannels with an aspect ratio of around one.[12,28] It is also shown that the aspect ratio of the channel is an importatnt factor to determine the success of the fabrication. The minimum aspect ratio of surviving channels is around 0.004, which is rather consistent for varying nanochannel depths from 180 nm down to 20 nm. Our experimental results do not conform to the criterion for the collapse of a microchannel developed by Shih *et al.*,[29] claiming that the collapse can be avoided as long as the ratio of the channel width to the cube of the depth of the channel is less than some constant associated with the applied voltage and material constant during anodic bonding. A more detailed model might be needed to establish the criterion for the collapse of nanochannels. It is not clear whether 20 nm is the ultimate minimum thickness that can be attained from this technique.

Table 1 Survival or collapse of the silicon–glass nanofluidic channels[a] after anodic bonding[b]

	Channel width/μm						
Channel depth/nm	3	5	10	20	50	200	Minimum aspect ratio[c]
180	Survive	Survive	Survive	Survive	Survive	Collapse	0.0036
80	Survive	Survive	Survive	Survive	Collapse	Collapse	0.004
40	Survive	Survive	Survive	Collapse	Collapse	Collapse	0.004
20	Survive	Survive	Collapse	Collapse	Collapse	Collapse	0.004

[a] The channels consist of 2 cm long parallel lines spaced by 5 μm. [b] Bonding condition: 6″ Borofloat glass; 390 nm oxide grown on <100> silicon wafers; 350 °C, 800 V; 2000 N pressure force; EV501 Bonder machine. [c] The ratio of the depth to the width of the channel.

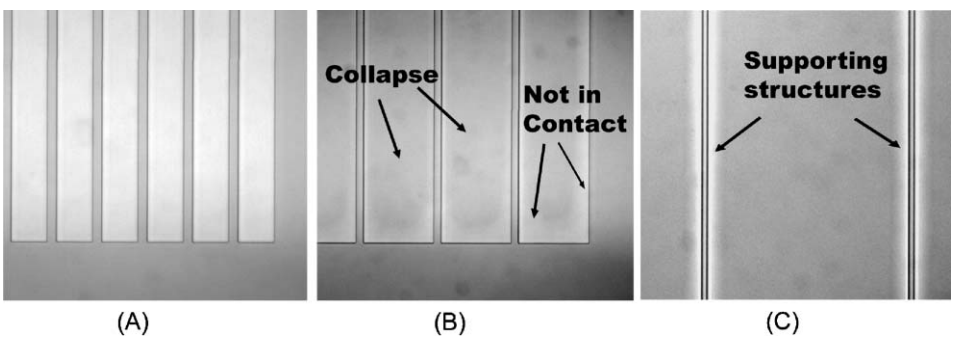

Fig. 4 Optical observation of the survival or collapse of the channels. (A) Survived channels with the depth of 80 nm and width of 20 μm, spaced by 5 μm. (B) Collapsed channels with the depth of 80 nm and width of 50 μm, spaced by 5 μm. Very small areas along the edge did not collapse. (C) The entire channels, 200 μm in width and 180 nm in depth, collapsed except along the edge. The channels turned from bright to gray when they collapsed.

We are still in the process of pushing this technique down to 10 nm or even thinner.

In addition, we succeeded in filling channels to make sure the nanochannels survived. Fig. 5 shows the fabricated 20 nm nanofluidic channels and the filling of the channel with concentrated FITC dye in TBE 5X buffer solution. Due to the strong capillary force, buffer solution as well as dye molecules were introduced to the 20 nm deep nanofluidic channel without any external driving force. It was possible to fill 1–2 cm long, 3 μm wide and 20 nm deep nanochannels within 20 minutes.

When the channel fabrication fails due to too small aspect ratio, usually the entire channel gets sagged. While the temperature for anodic bonding is much lower than the glass transition temperature (~550 °C), the applied electrical field exerts a strong force between the walls of the nanochannel during the bonding process. If the aspect ratio is smaller than a certain critical number, bending of the substrates could cause the contact between the top and bottom surfaces, which will be bonded instantly and permanently at this condition. Once a small contact area is formed, it will quickly expand across the entire device, thus leading to complete contact between the top and bottom walls of the nanochannel. In that sense, decreasing the bonding potential and temperature might achieve better success for fabricating nanochannels with lower aspect ratio, but this is yet to be tested.

All the thickness of nanochannels shown above was measured by using Tencor P-10 surface profilometer (with vertical resolution less than 5 Å) before the anodic bonding step. Scanning electron microscopy (SEM) imaging was performed to measure and confirm the thickness of nanofluidic channels after the bonding process. The cross-sectional SEM images of nanochannels with various depths are shown in Fig. 6. It can be seen that the channels are of good uniformity and completely open, and there is no significant deformation or sagging of the nanochannels, even for 20 nm deep channels. The comparison of the nanochannel depths measured from the profilometer (before bonding) and SEM (after bonding) shows

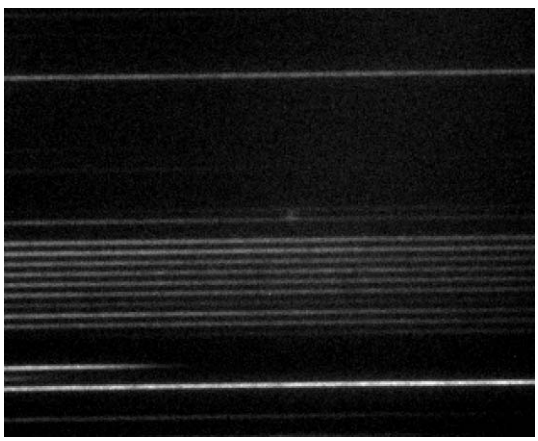

Fig. 5 Fluorescence imaging of 20 nm deep nanofluidic channels being filled with concentrated FITC dye in TBE 5X buffer solution. Due to a strong capillary force, buffer solution as well as dye molecules spontaneously filled the entire nanofluidic channel without any external driving force. The channels are 3 μm wide spaced by 3 μm.

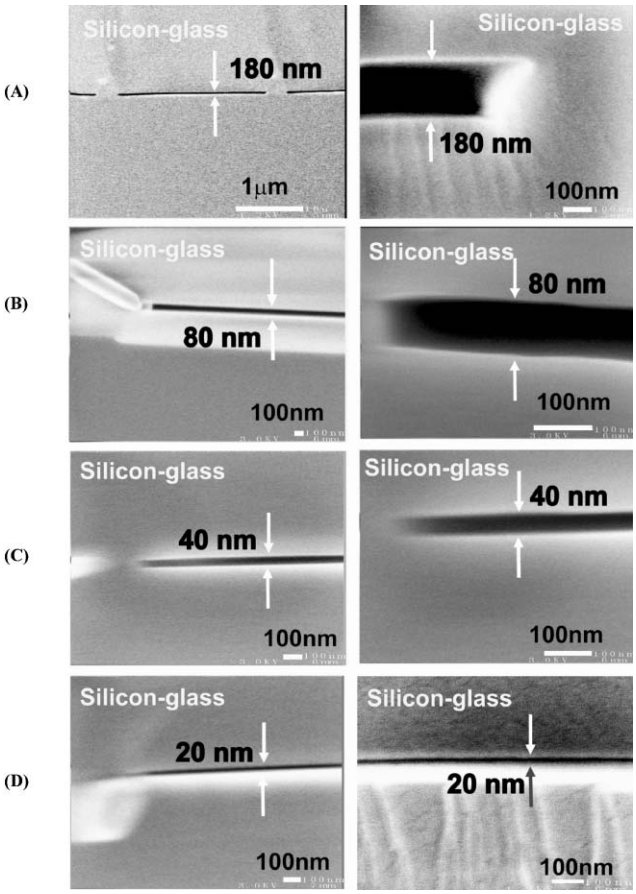

Fig. 6 Cross-sectional SEM images and close-up of nanochannels with various depths of 180 nm (A), 80 nm (B), 40 nm (C), and 20 nm (D) on silicon substrate (bottom wafer) bonded to a borofloat wafer (top wafer), respectively.

that no statistically significant change of the depth caused by the bonding process can be observed, within the 10% possible error due to limited resolution of SEM images. The other possible errors for the difference may be the nonuniformity of RIE etching over the whole wafer and Au coating for SEM imaging. Hence, it is proven that the anodic bonding process in our bonding condition causes little change in the depth of the nanochannel, if the proper aspect ratio of the channel is maintained.

Nanochannel fabrication by glass–glass fusion bonding

We use direct glass–glass bonding (thermal fusion) to seal the channels. The important factors affecting successful thermal fusion bonding of glass wafers include the cleanness of the bonding glass surface, surface flatness of glass substrates, bonding temperature, and pressure. Our experimental results support the assumption that the glass substrates might be joined by hydrogen bond formation when brought into contact at room temperature.[20] We found that about 70%~80% bonded areas (6″ wafer area) were achieved due to this weak hydrogen bonding. Permanent bonding was achieved by annealing glass substrates at high temperature. We found that relatively weak bonding was formed in a temperature less than 500 °C, which could not withstand the cutting process with a

diamand cutter, even though glass substrates were annealed for quite a long time. We chose 550 °C as annealing temperature, which is approximately equal to the glass transition temperature for Pyrex. At this temperature, strong bonding between the two glass substrates was produced with 100% bonding yield and the bonded areas were increased to 90%–95% after annealing. Although no apparatus was used to determine the exact bonding strength, it was found that the bonded chips could withstand the cutting and breaking process, and there was no fluid permeation around the channel when a dye solution was introduced into the channel by applying an electric field of 300 V cm^{-1}. Hence, we believe that considerably strong, permanent bonding between glass substrates at 550 °C has been achieved to fabricate nanofluidic glass chips. The annealing at temperature above 550 °C might accomplish stronger bonding, but a glass material might melt and deform at higher temperatures and nanochannels might collapse. For example, Fan and Harrison found that 1 mm wide, 10 μm deep channels made of Pyrex at 650 °C collapsed.[26] Therefore, bonding temperature might have a dramatic effect on the minimum depth and aspect ratio that can be achieved without collapse, which will be investigated in the future. An appropriate temperature program with controlled ramping and cooldown rates is also important. The fabrication process on glass substrate we develop is quite simple and reproducible, and can be used widely since it does not require specific, expensive tools.

Table 2 summarizes the results of bonded channels with various widths and depths by optical inspection. Nanochannels as deep as 25 nm on glass substrate with aspect ratio of 0.0005 have been achieved reliably. This aspect ratio is much smaller than the one (0.004) obtained for silicon–glass channels by using the anodic bonding technique. In addition, we have succeeded in pushing the thickness of nanochannels down to 15 nm, but a higher aspect ratio of 0.015 is required to fabricate non-collapsing channels. The optical image of the 15 nm deep nanochannel with a width of 3 μm is shown in Fig. 7(B). It can be seen that nanochannels collapse in some regions but survive in the other regions, which is different from the collapsing behavior in the silicon–glass nanochannels where the channels completely collapse except along the edge. This is probably because we are not exerting a strong external force to push the two interfaces together as in anodic bonding. While this allows nanochannels with lower aspect ratio to be fabricated, the weak bonding force decreases the bonding area slightly ($\sim$95% bonded surface area instead of $\sim$100% bonded surface area in anodic bonding).

Fig. 8 shows the surface profile of an etched glass channel in buffed HF for 30 s by using an atomic force microscope (Nanoscope IIIa, Digital Instruments). The average surface roughness (R_a) is around 1.3 nm inside a 2.0 × 2.0 μm^2 scanned area, which is comparable to the original surface flatness (guaranteed by the manufacturer) of glass material we use. Therefore, the short etching process does not increase (local) surface roughness singificantly. Given the pattern of collapsed regions in the 15 nm nanochannel fabrication, we would think that the long range thickness variation of the glass substrate (around tens of microns) might have caused the failure. However, the underlying mechanism of collapse remains to be investigated by careful experimental characterization as well as theoretical analysis. Due to the specification of the Pyrex glass material and surface roughness resulting

Table 2 Survival or collapse of the glass–glass nanochannels consisting of 2 cm long parallel lines spaced by 5 μm after direct glass–glass bonding[a]

	Channel width/μm						
Channel depth/nm	1	3	10	20	50	100	Minimum aspect ratio[b]
100	Survive	Survive	Survive	Survive	Survive	Survive	<0.001
55	Survive	Survive	Survive	Survive	Survive	Survive	<0.00055
25	Survive	Survive	Survive	Survive	Survive	Collapse	0.0004
15	Survive	Collapse	Collapse	Collapse	Collapse	Collapse	0.015

[a] Bonding condition: Pyrex glass (6″, 500 μm thick, double sides polished); Annealing was performed for 14 hours at 550 °C with a ramp rate of 1.5 °C min^{-1} and a cooldown rate of 2.0 °C min^{-1} and no applied pressure in a programmable box furnace. [b] The ratio of the depth to the width of the channel.

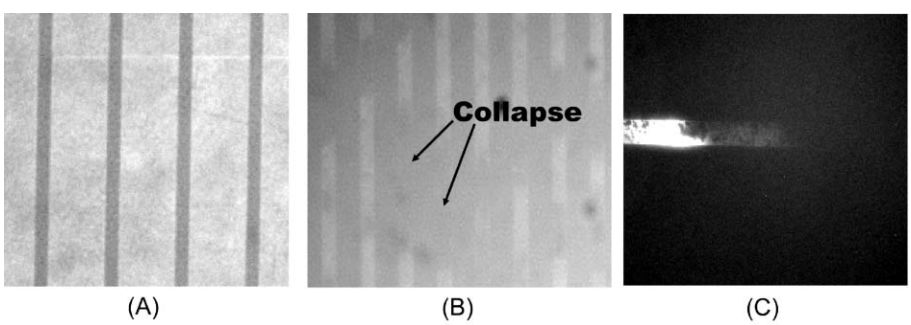

Fig. 7 Optical micrograph of glass nanochannels. (A) 10 μm wide and 25 nm deep nanochannels survived after bonding. (B) 3 μm wide and 15 nm deep nanofluidic channels collapsed. (C) Fluorescence imaging of 30 nm deep glass fluidic channels, 30 μm in width, being filled with 20 μM Alexa Fluro 488-labeled 18-mer DNA oligos in TBE 5X buffer solution.

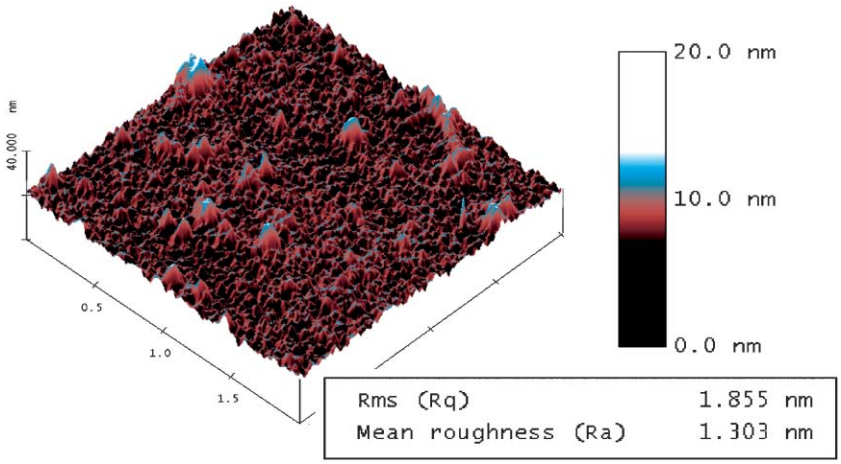

Fig. 8 Surface profile of a glass channel etched for 30 s in BOE (7:1) without agitation, using atomic force microscopy. The surface roughness is around 1.3 nm.

from the wet etching process, we believe that 20 nm would be the minimum thickness to be achieved with this fabrication technique at 550 °C for a wide range of aspect ratio without collapse.

Due to the potential flow of glass material at high bonding temperature, there is a concern that the actual thickness of nanochannels after bonding might be different from the thickness measured by surface profilometer before bonding, especially since the bonding temperature is close to the glass transition temperature of the Pyrex glass. SEM imaging was performed to investigate this issue. The cross-sectional SEM images of nanochannels with various depths are shown in Fig. 9. The etched channels are completely open and retain their original shape with good uniformity, and even the undercut from the wet etching process can be observed. In addition, no interface is visible between the two glass substrates. It is found out that the thickness of the channels measured by SEM imaging after bonding is almost equal to the thickness before bonding, within ~10% possible error caused by SEM image analysis. Therefore, there is no significant change of the depth due to the fusion bonding process at 550 °C.

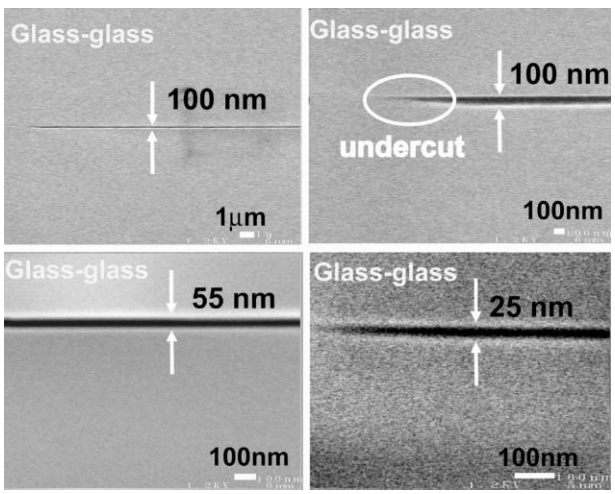

Fig. 9 Cross-sectional SEM images of nanochannels with depths of 100 nm, 55 nm and 25 nm fabricated on glass substrate bonded with another glass cover.

Conclusions

We have fully characterized both Si–glass anodic bonding and glass–glass fusion bonding processes for the fabrication of wide, shallow planar nanofluidic channels as thin as 20 nm. We have demonstrated that nanofluidic channels, as thin as 20 nm with aspect ratio (1:250, depth to width) on silicon substrate and 25 nm with aspect ratio of 0.0005 on glass substrate can be achieved with anodic bonding technique and developed glass–glass bonding technique, respectively. Cross-sectional SEM analysis has proved that there is no significant change of the depth of nanofluidic channels due to the anodic bonding process and the glass–glass bonding process. The aspect ratio of the planar nanochannels achieved in this work (0.004 ~ 0.0002) is small enough, so that standard photolithography (with typical lateral patterning resolution of >1 μm) can be used to generate nanofluidic channels as thin as 20 nm. The availability of such a uniform, flat nanofluidic channel could lead to more careful, controlled study of molecular and fluidic transport in nanopores or confined space. This result will be useful in designing next-generation nanofluidic devices that can be used for protein separation[3] and biomolecule preconcentration.[30]

Acknowledgements

The authors gratefully acknowledge financial support from MIT Lincoln Laboratory (ACC 353), National Science Foundation NSE (CTS-0304106) and CAREER program (CTS-0347348). We would like to thank Jianping Fu and Ying-Chih Wang for valuable input and discussion, and Dr Jeroen Haneveld for suggestions for cutting wafers and SEM imaging. We also thank the staff in the Microsystems Technology Laboratoreies (MTL) of MIT for assistance in device fabrication.

References

1 J. Han, in *Nanofluidics*, ed. M. D. Ventra, S. Evoy and J. R. Heflin, 2004.
2 J. Han and H. G. Craighead, *Science*, 2000, **288**, 1026.
3 J. Fu and J. Han, in *Proceedings of the 2004 Micro Total Analysis Systems International Conference*, Malmö, Sweden, 2004, p. 285.
4 P. M. Sinha, G. Valco, S. Sharma, X. Liu and M. Ferrari, *Nanotechnology*, 2004, **15**, S585.
5 O. A. Saleh and L. L. Sohn, *Rev. Sci. Instrum.*, 2001, **72**, 4449.
6 O. A. Saleh and L. L. Sohn, *Nano Lett.*, 2003, **3**, 37.
7 M. Foquet, J. Korlach, W. Zipfel, W. W. Webb and H. G. Craighead, *Anal. Chem.*, 2002, **74**, 1415.
8 M. Foquet, J. Korlach, W. R. Zipfel, W. W. Webb and H. G. Craighead, *Anal. Chem.*, 2004, **76**, 1618.
9 O. B. Bakajin, T. A. J. Duke, C. F. Chou, S. S. Chan, R. H. Austin and E. C. Cox, *Phys. Rev. Lett.*, 1998, **80**, 2737.
10 Y.-L. Chen, M. D. Graham, J. J. d. Pablo, G. C. Randall, M. Gupta and P. S. Doyle, *Phys. Rev. E*, 2004, **70**, 60901.
11 S. W. Turner, A. M. Perez, A. Lopez and H. G. Craighead, *J. Vac. Sci. Technol., B*, 1998, **16**, 3835.
12 H. Cao, Z. Yu, J. Wang, J. O. Tegenfeldt, R. H. Austin, E. Chen, W. Wu and S. Y. Chou, *Appl. Phys. Lett.*, 2002, **81**, 174.
13 J. R. Webster, M. A. Burns, D. T. Burke and C. H. Mastrangelo, *Anal. Chem.*, 2001, **73**, 1622.
14 J. O. Tegenfeldt, C. Prinz, H. Cao, S. Chou, W. W. Reisner, R. Riehn, Y. M. Wang, E. C. Cox, J. C. Sturm, P. Silberzan and R. H. Austin, *Proc. Natl. Acad. Sci. U.S.A.*, 2004, **101**, 10979.
15 J. Kasianowicz, E. Brandin, D. Branton and D. Deamer, *Proc. Natl. Acad. Sci. U.S.A.*, 1996, **93**, 13770.
16 J. Han and H. G. Craighead, *J. Vac. Sci. Technol., A*, 1999, **17**, 2142.
17 J. Han and H. G. Craighead, *Anal. Chem.*, 2002, **74**, 394.
18 G. Wallis and D. I. Pomerantz, *J. Appl. Phys.*, 1969, **40**, 3946.
19 J. Han, *Entropic Trap Array Device for DNA separation*, *PhD*, Cornell University, Ithaca, NY, 2001.
20 H. Y. Wang, R. S. Foote, S. C. Jacobson, J. H. Schneibel and J. M. Ramsey, *Sens. Actuators, B*, 1997, **45**, 199.
21 Z. Huang, J. C. Sanders, C. Dunsmor, H. Ahmadzadeh and J. P. Landers, *Electrophoresis*, 2001, **22**, 3924.
22 A. Sayah, D. Solignac, T. Cueni and M. A. M. Gijs, *Sens. Actuators, B*, 2000, **84**, 103.
23 N. Chiem, L. Lockyear-Shultz, P. Andersson, C. Skinner and D. J. Harrison, *Sens. Actuators, B*, 2000, **63**, 147.
24 Z.-j. Jia, Q. Fang and Z.-L. Fang, *Anal. Chem.*, 2004, **76**, 5597.
25 C.-H. Lin, G.-B. Lee, Y.-H. Lin and G.-L. Chang, *J. Micromech. Microeng.*, 2001, **11**, 726.
26 Z. H. Fan and D. J. Harrison, *Anal. Chem.*, 1994, **66**, 177.
27 J. L. Vossen and W. Kern, *Thin Film Processes*, Academic Press, 1978.
28 S. W. Turner, A. M. Perez, A. Lopez and H. G. Craighead, *J. Vac. Sci. Technol., B*, 1998, **16**, 3835.
29 W.-P. Shih, C.-Y. Hui and N. C. Tien, *J. Appl. Phys.*, 2004, **95**, 2800.
30 Y.-C. Wang, A. L. Stevens and J. Han, *Anal. Chem.*, 2005, DOI: 10.1021/ac050321z.